

# Millimeter-Scale Magnetic Swimmers Using Elastomeric Undulations

Jiachen Zhang and Eric Diller

**Abstract**—This paper presents a new soft-bodied millimeter-scale swimmer actuated by rotating uniform magnetic fields. The proposed swimmer moves through internal undulatory deformations, resulting from a magnetization profile programmed into its body. To understand the motion of the swimmer, a mathematical model is developed to describe the general relationship between the deflection of a flexible strip and its magnetization profile. As a special case, the situation of the swimmer on the water surface is analyzed and predictions made by the model are experimentally verified. Experimental results show the controllability of the proposed swimmer under a computer vision-based closed-loop controller. The swimmers have nominal dimensions of  $1.5 \times 4.9 \times 0.06$  mm and a top speed of 50 mm/s (10 body lengths per second). Waypoint following and multi-agent control are demonstrated for swimmers constrained at the air-water interface and underwater swimming is also shown, suggesting the promising potential of this type of swimmer in biomedical and microfluidic applications.

## I. INTRODUCTION

Untethered mobile microrobots have the potential for application in many biomedical areas, because they can access small, constrained environments to perform tasks such as cargo delivery and object manipulation [1]–[3]. It is an ongoing challenge in the community to design effective and efficient approaches to remotely actuate and control these microrobots, due to the fabrication and control limitations at the sub-millimeter scale. Different methods for remote actuation and control of these devices have been proposed, including strategies using biological microorganisms [4], chemical reactions [5], electrical substrates [6], and magnetic fields [7]–[14]. Among these techniques, the use of magnetic fields has become a common choice to wirelessly actuate and control microrobots in fluidic environments, resulting from the fact that magnetic fields can penetrate most materials and generate forces and torques on microrobots independently or simultaneously. Many of the methods using magnetic fields employ similar field generation setups, which opens the possibility of controlling different microrobots using the same setup, and promotes the application of these microrobots by reducing the implementation cost.

Under some conditions, it is shown in [15] that magnetic torques resulting from uniform magnetic fields is a preferable option over magnetic forces generated by magnetic gradients for driving a magnetic device at sub-millimeter scale in a liquid medium. Utilizing magnetic torques, several locomotion strategies have been proposed to actuate microrobots in a swimming gait [9]–[14]. Such swimmers have gained a large

amount of attention as the result of their promising potential of high efficiency and easy control. Some of these swimmers have soft bodies, which offer gentle interactions with the environment and are especially suitable for many biomedical applications [12]–[14]. The concept of a soft-bodied swimmer propelled by the propagation of a lateral traveling waves along its body has been explored in [16], [17]. However, [16] provides no experimental demonstrations, while the swimmer discussed in [17] is at the scale of centimeter. In addition, both of the swimmers require embedded actuators such as on-board batteries or wired power supply, which limit their potential to be further scaled down.

This paper presents a new soft-bodied millimeter-scale swimmer that is wirelessly actuated by rotating uniform magnetic fields. The swimmer moves through internal undulatory deformations, resulting from a unique magnetization profile programmed into its body. The concept of this swimmer was reported in [14] with a limited demonstration of motions and swimming speed measurements. Here we present a mathematical model to describe the relationship between the swimmer's deflection and magnetization profiles, and show the controllability of the swimmer using an accurate computer vision-based closed-loop controller for robotics and automation applications. Waypoint following and multi-swimmer control are demonstrated for swimmers constrained at the air-water interface, and underwater swimming is also shown.

## II. CONCEPT AND MATHEMATICAL MODEL

The proposed swimmer consists of a flexible magnetic strip modeled as a two-dimensional (2D) body. This strip is placed in uniform magnetic fields for remote actuation and control, which induce deflections in the magnetic strip. By programming a specific magnetization profile into the strip, the desired deflection profile can be achieved, which make the strip swim. To study the swimming motion of the strip in this work, it is placed at the air-water interface to constrain its motion to a plane. The relevant physical forces acting on the strip in this case include internal elastic forces, magnetic torques applied from the external magnetic field, and interaction forces with the environment such as capillary and fluid propulsion forces. This section presents a mathematical model of the proposed swimmer, starting with a general elastic-magnetic bending model of a flexible 2D strip in uniform magnetic fields. Next we model the physical conditions acting on a swimmer resting on or under the water surface, and introduce a model for its swimming speed.

\*This work is supported by the NSERC Discovery Grants Program.

J. Zhang and E. Diller are with the department of Mechanical and Industrial Engineering, University of Toronto, 5 King's College Road, Canada ediller@mie.utoronto.ca

### A. Elastic-Magnetic Bending Model

A flexible strip with a magnetization profile varying along its long axis experiences distributed torques in uniform magnetic fields, which can be calculated by

$$d\boldsymbol{\tau} = \mathbf{M}(x) \times \mathbf{B} A dx, \quad (1)$$

where  $d\boldsymbol{\tau}$  is the distributed torque (torque per length),  $\mathbf{M}$  is the magnetization,  $\mathbf{B}$  is the external magnetic field,  $A$  is the cross-sectional area of the strip, and  $x$  is the coordinate of the position along the strip's long axis. The bending moment  $Q(x)$  caused by magnetic torques is determined by

$$Q(x) = - \int_0^x d\boldsymbol{\tau}. \quad (2)$$

When the deflection is small, the bending moment can be expressed by the Euler-Bernoulli equation as

$$Q = EI \frac{d^2\omega}{dx^2}, \quad (3)$$

where  $E$  and  $I$  are the strip's Young's modulus and second moment of area, respectively. The deflection profile of the strip is denoted as  $\omega(x)$ , which can be solved from (1), (2) and (3) with a known magnetization profile, appropriate boundary conditions, and no other forces or torques involved. It is also possible to calculate the magnetization profile required for a desired deflection profile, under particular boundary conditions.

### B. Swimmer Model

When a strip with a magnetization profile is placed in a rotating uniform magnetic field, its deflection will change continuously and periodically. Among the infinite number of profiles possible, the sinusoidal magnetization profile generates an approximate traveling wave along the strip at the air-water interface in rotating magnetic fields. This traveling wave propels the strip and makes it move in a swimming gait. Thus the strip with a sinusoidal magnetization profile is referred to as the swimmer hereafter. The sinusoidal magnetization profile is represented by

$$\mathbf{M}(x) = M \cos\left(\frac{2\pi x}{\lambda}\right) \mathbf{i} + M \sin\left(\frac{2\pi x}{\lambda}\right) \mathbf{j}, \quad (4)$$

where  $M$  is the magnetization magnitude,  $\lambda$  is the wavelength of the sinusoidal magnetization profile, and  $\mathbf{i}$  and  $\mathbf{j}$  are the unit vectors along the positive directions of  $x$  and  $y$  axes, respectively. This magnetization profile can be created by rolling the strip into a circle and placing it in a magnetizing field, as illustrated in Fig. 1. The two configurations shown in Fig. 1(a,b) will be further discussed in Section III.

After magnetization, the swimmer experiences distributed torques when placed in a rotating magnetic field in the  $x$ - $y$  plane. Defining  $\alpha$  as the angle from the swimmer's geometric heading (positive  $x$  axis) to the external magnetic field with counter-clockwise as its positive direction, the deflection of the swimmer can be solved from (1), (2) and (3) as

$$\omega(x, \alpha) = \frac{MAB\lambda^3}{8\pi^3 EI} a + \frac{MAB\lambda}{2\pi EI} b + c, \quad (5)$$

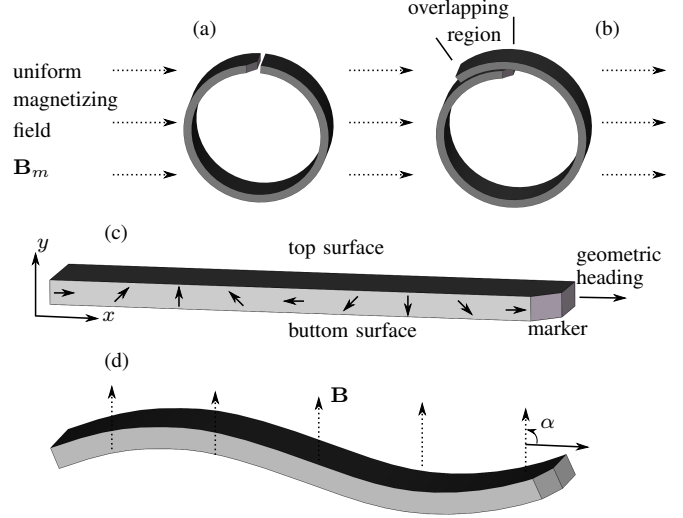


Fig. 1. Schematics of the setup to program a sinusoidal magnetization profile into the swimmer's body. A small chamfer is made on one corner to mark the swimmer's heading. Two configurations of the setup for magnetizing the swimmer are shown in (a) and (b), with the difference that the configuration in (b) has an overlapping region to induce the direction of the net magnetization to a  $\pm 5^\circ$  range near the swimmer's geometric heading. The resultant magnetization profile and the swimmer's deflection in a uniform magnetic field are shown in (c) and (d), respectively.

where

$$a = \cos\left(\frac{2\pi x}{\lambda} - \alpha\right),$$

$$b = \frac{x^2}{2} \cos \alpha - \frac{\lambda x}{2\pi} \sin \alpha - \frac{\lambda^2}{4\pi^2} \cos \alpha,$$

and

$$c = \frac{1}{2EI} Q(0)x^2 + k(0)x + \omega(0).$$

Here  $Q(0)$ ,  $k(0)$ , and  $\omega(0)$  are the values of the bending moment, slope, and deflection at the point of  $x = 0$ , respectively. Because there are other terms besides the sinusoidal term  $a$  in  $\omega(x, \alpha)$ , the shape of the swimmer is not a perfect sinusoidal wave. However, when the swimmer moves at the air-water surface, an approximated traveling sinusoidal wave is generated along the swimmer's body, under the combined effect of magnetic torques, surface tension forces and buoyancies. It is shown in [18] that the vertical component of the surface tension force experienced by a partly submerged object equals the weight of liquid displaced by the meniscus caused by this object. This result indicates that the vertical component of the surface tension force experienced by the swimmer is a function of the fluid density, gravitational acceleration, and  $\omega$ . Based on this result, a phenomenological model in the form of an exponential equation is built to approximate the vertical component of the surface tension force within the concerned range of deflection as

$$dF_t = \rho g \cdot \text{sgn}(\omega) |\omega|^{1.4} dx, \quad (6)$$

where  $\rho$  and  $g$  are the density of water and the gravitational acceleration, respectively. The exponent value in (6) is obtained by fitting deflection measurements of the swimmer

with the model employing this exponential form. Therefore (6) is expected to give a reasonable estimation only when the deflection is within the range concerned in this work. Besides the surface tension force, the vertical component of the buoyancy experienced by the swimmer is

$$dF_p = \rho g c \omega dx, \quad (7)$$

where  $c$  is the width of the swimmer's cross section.

Because the surface tension force and buoyancy experienced by the swimmer are distributed along the swimmer's entire length, the deflection profile of the swimmer on the water surface is calculated iteratively. While no closed-form solution exists for the deflection under these boundary conditions, the deflection profile of the swimmer closely resembles a sinusoidal wave, as will be verified experimentally in Section IV. Under different boundary conditions, the swimmer assumes different deflection profiles even though its magnetization profile is not changed. For example, the swimmer's deflection profile is distinctly different when it moves under the water surface, which deviates from a sinusoidal wave and hinders its swimming behavior.

With its inertia ignored, the continuously changing deflection profile of a swimmer in rotating magnetic fields can be approximated as a traveling wave, which is similar with the undulating waves created on the surface of ciliates. The swimming speed of the swimmer is modeled based on a formulation presented in [19] as

$$V = \frac{2\pi^2 b^2}{\lambda} f, \quad (8)$$

where  $V$ ,  $b$ ,  $\lambda$ , and  $f$  are the velocity of the sheet, the amplitude of the wave, the wavelength, and the wave frequency, respectively. It is worth noting that this model is developed for an inextensible sheet propelled by waves with small amplitude in a viscous fluid. Even though the proposed swimmer does not fit all the assumptions made for (8), this equation characterizes the basic relationship between the swimmer's speed and the deflection amplitude and frequency, which is shown in [14]. The approximate traveling wave generated along the swimmer's body in a rotating magnetic field propels the swimmer to move along its long axis, whose speed can be characterized using (8).

### III. CONTROL ALGORITHM AND EXPERIMENTAL SETUP

The swimmer moves under the influence of an out-of-plane rotating magnetic field (actuation field  $\mathbf{B}_a$ ) for propulsion and a small constant in-plane magnetic field (bias DC field  $\mathbf{B}_{dc}$ ) that controls orientation. This section presents an algorithm and the experimental setup to control the planar speed and orientation of a prototype swimmer in real-time.

#### A. Control Algorithm

The swimmer, constrained at the air-water interface, swims in a non-holonomic fashion (forwards and backwards) in the plane, propelled by  $\mathbf{B}_a$  and steered by  $\mathbf{B}_{dc}$ . The steering field acts to bring the net magnetization vector into alignment with the field. For swimmers magnetized into a single-period sinusoid as in Fig. 1(a), their net magnetization

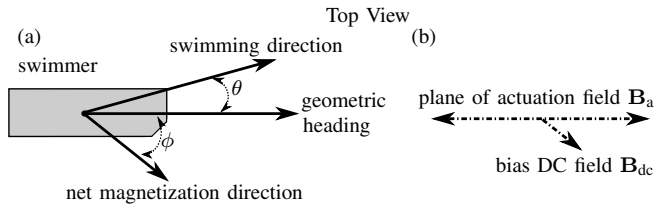


Fig. 2. Angles related to the swimming behavior and the orientation of the actuation and bias DC fields. (a) Angle  $\phi$  defines the orientation of the net magnetization direction while angle  $\theta$  defines the swimming direction. (b) The actuation field plane and the net magnetization direction align with the swimmer's heading and the bias DC field, respectively.

sums to zero. Thus, the only net magnetization is due to fabrication and magnetization imperfections and its direction cannot be oriented. To control the net magnetization, a small "overlapping region" can be added during the magnetization step, as shown in Fig 1(b), which leads to a net magnetization direction approximately aligned with the geometric heading of the swimmer. Angles related to the swimming behavior of the proposed swimmer are defined in Fig. 2. The frequency of  $\mathbf{B}_a$  is fixed at 30 Hz in the proposed control algorithm. At this frequency, unwanted oscillation of the swimmer caused by  $\mathbf{B}_a$  is well suppressed, and the swimming angle  $\theta$  is always smaller than one degree, which is considered as zero for simplification. To maximize the propelling efficiency of  $\mathbf{B}_a$ , its plane is always aligned with the swimmer's long axis, as shown in Fig. 2.

As indicated by (8), the swimmer's speed is proportional to its deflection's amplitude square and frequency, which can be controlled by the amplitude and frequency of  $\mathbf{B}_a$ , respectively. With its frequency fixed at 30 Hz, the amplitude of  $\mathbf{B}_a$  is used by the control system to control the swimmer's speed. A second part of the control system is responsible for the swimmer's orientation. This part steers the swimmer by changing the direction of  $\mathbf{B}_{dc}$  based on the desired heading and  $\phi$ , which is measured and updated by the controller in real-time. The magnitude of  $\mathbf{B}_{dc}$  is a fixed percentage of the amplitude of  $\mathbf{B}_a$ . Based on the information of the swimmer's present position and heading acquired from visual feedback, the amplitude of  $\mathbf{B}_a$  and the direction of  $\mathbf{B}_{dc}$  are controlled in real-time, using a proportional (P) controller and a proportional-integral (PI) controller, respectively, as shown in Fig. 3. The P controller for the swimming speed has a dead zone and a saturation value, which are implemented to limit the swimmer's speed within a reasonable range. The input to this controller is the goal position  $\mathbf{X}_d$ , which can be specified by the user or a higher level automated controller. Considering the swimmer can only swim along its long axis, the swimmer will be steered first before being actuated to swim, when a new goal point is specified and the line connecting the swimmer's center point and its new goal point does not align with the swimmer's geometric heading.

#### B. Experimental Setup

The swimmer is made from unmagnetized permanent magnetic particles (MQFP-15-7, NdPrFeB, Magnequench)

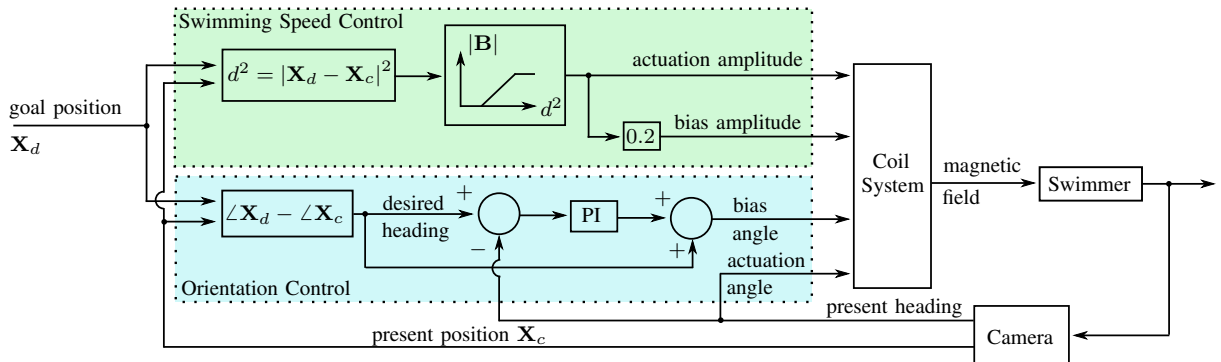


Fig. 3. Block diagram of the computer vision based feedback control system for the proposed swimmer. This control algorithm controls the swimming speed and direction of the swimmer through the actuation amplitude, actuation angle, bias amplitude, and bias angle.

and highly flexible elastomer (Ecoflex 00-50, density  $1.07 \text{ g/cm}^3$ , Young's modulus  $83 \text{ kPa}$ ). The magnetic particles, with diameter around  $5 \mu\text{m}$ , are mixed with the elastomer at a mass ratio of 1:1. The mixture is pressed between two plates during its curing process, resulting in a thickness of  $60 \mu\text{m}$ , determined by spacers. The swimmer is manually cut from the sheet with nominal dimensions of  $1.5 \times 4.9 \text{ mm}$ . Next, the swimmer is rolled into a circle and placed in a uniform magnetizing field ( $1 \text{ T}$ ) that is perpendicular to the axis of the circle, as shown in Fig. 1(a). After the swimmer is removed from the magnetizing field and unrolled, it has a sinusoidal magnetization profile with amplitude  $M = 48 \text{ kA/m}$  along its body, as shown in Fig. 1(c).

Experiments are performed using an electromagnetic coil system shown in Fig. 4, a current generating system of three analog servo drives (30A8, Advanced Motion Controls) for the three pairs of wire in the coil system, and custom codes running on a computer with a multifunction analog/digital I/O board (Model 826, Sensoray) installed. Feedback information is provided by a top-view camera (FO134TC, FOculus) running at  $60 \text{ fps}$ . Each pair of wire in the coil system is arranged to approximate a Helmholtz coil. The coil system is capable of generating a uniform field ( $\pm 5\%$ ) up to  $15 \text{ mT}$  in arbitrary 3D directions near its geometric center, within a sphere with a diameter of  $44 \text{ mm}$ .

#### IV. EXPERIMENTS

This section provides experimental data to verify the proposed model describing the deflection profile of the swimmer on the water surface, demonstrate the controllability of the proposed swimmer under feedback control for precise waypoint following, and manifest the swimmer's potential for multi-agent control.

##### A. Model Verification

The swimmer with dimensions of  $1.46 \times 4.86 \text{ mm}$  rested on the water surface in a container, which was placed in a uniform magnetic field of  $4 \text{ mT}$ . Fig. 5 shows a comparison between the deflection measurements and the predictions, which were calculated by the proposed model with the boundary conditions that the net force and the bending moments at both ends of the swimmer are all zero. The average

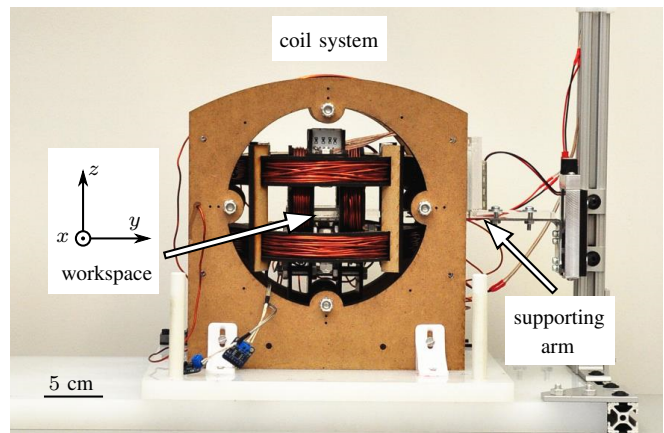


Fig. 4. Photograph of the electromagnetic coil system. The coordinate frame of the workspace is labeled in this picture. A top-view camera (not shown) is mounted above the workspace, pointing towards the negative  $z$  direction.

root-mean-square (rms) value of the differences between the experimental data and predictions for the four cases shown in Fig. 5 is  $31 \mu\text{m}$ . The small rms value suggests a good agreement between the predictions made by the proposed mathematical model and the experimental measurements, which proves the accuracy of the model within the concerned range of deflection.

##### B. Two-Dimensional Waypoint Following

Employing the proposed feedback control algorithm, a swimmer can be controlled to automatically follow a pre-specified sequence of waypoints. To demonstrate this, three swimmers with similar dimensions were controlled to follow the waypoints defined by the corners of the two letters "U" and "T". The closed-loop control system specified the seven way points as a sequence of goal points for the swimmer to reach. The average completion time and deviation of each swimmer for three trials are listed in Table I, and a trial of this experiment is shown in Fig. 6.

Even having different net magnetization directions, all three swimmers followed the sequence of waypoints with a certain accuracy, which manifests the controllability of the proposed swimmer and the capacity of the developed

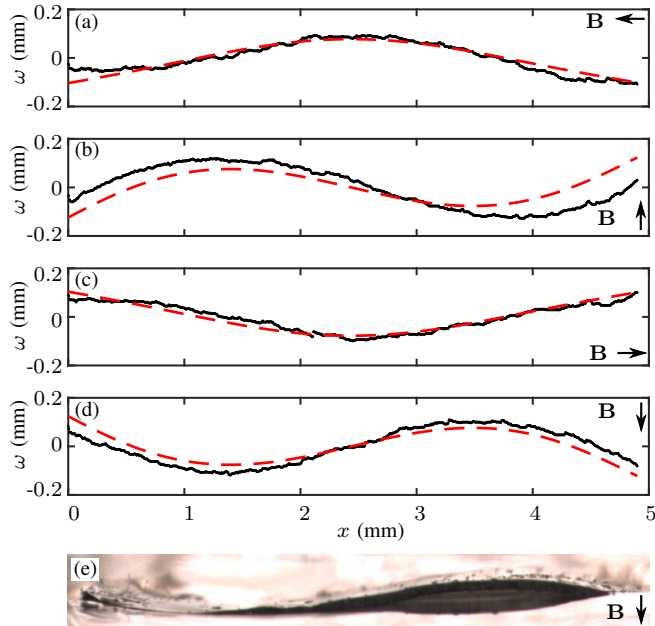


Fig. 5. Deflection profiles of the swimmer resting on the water surface in magnetic fields of 4 mT in different directions. The predictions (dashed line) made by the proposed model are plotted together with the experimental measurements (solid line) in (a)-(d). Measurements are shifted vertically to fit the predictions. An image of the swimmer under a vertical magnetic field is shown in (e), whose data is shown in (d).

TABLE I  
SWIMMERS' PERFORMANCE IN WAYPOINT FOLLOWING EXPERIMENT

Swimmer	Dimensions (mm)	$\phi$ (deg.)	Completion Time (s)	Deviation RMS (body length)
A	$1.46 \times 4.86$	-79	11.08	0.10
B	$1.52 \times 4.86$	154	11.82	0.09
C	$1.47 \times 5.20$	19	9.94	0.05

computer vision-based closed-loop control system. It is worth noting that the parameters of the closed-loop control algorithm were not optimized, and the swimmer's speed was intentionally limited for convenience in control.

### C. Independent Control of Two Swimmers

As a result of the swimmer's non-holonomic swimming fashion, the swimmer will not move if the plane of  $\mathbf{B}_a$  is perpendicular to its heading. Employing this characteristic, swimmers with different geometric headings can be controlled to exhibit distinct swimming patterns in the same magnetic field. As a demonstration, two swimmers were fabricated, one of which (swimmer A) has a  $\phi$  value near zero, and angle  $\phi$  of the other swimmer (swimmer B) is near  $90^\circ$ . These two swimmers were controlled by the same magnetic field and frames of this experiment are shown in Fig. 7. This experiment shows that swimmer A and B were controlled in an independent but coupled fashion, meaning that they could move independently (0-8 s) or swim simultaneously in any combinations of forward and backward motions (8-24s).

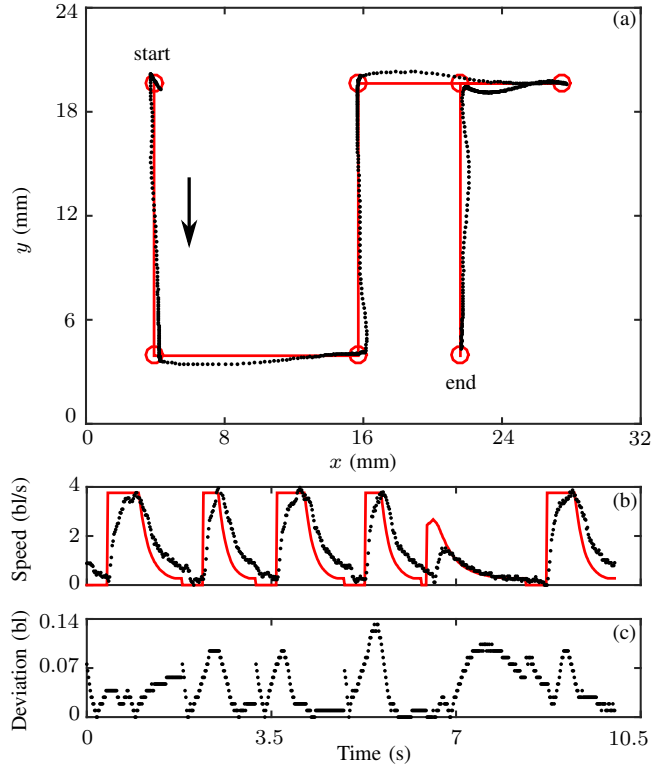


Fig. 6. Path of swimmer C and its speed and deviation data in one trial of the waypoint following experiment. Dots represent experimental data, while circles and lines are specified waypoints and expected path and values, respectively. The unit "bl" stands for the body length of the swimmer. Path of swimmer C is shown in (a). The experimental values of normalized speed are shown in (b) together with the expected values, which are calculated by the swimming speed controller based on the swimmer's distance to its destination. The normalized deviation of the swimmer is shown in (c). Video is available in supplementary materials.

These two swimmers could be steered by changing the direction of  $\mathbf{B}_{dc}$ . However, the relative orientation of the two swimmers' geometric headings is a fixed value, based on the difference between their  $\phi$  values. This experiment demonstrates the promising potential of the proposed swimmer for multi-agent control in tasks requiring a team of swimmers.

### D. Swimming Under the Water Surface

In addition to being able to swim on the water surface, the proposed swimmer can also swim under the water surface. However, with the absence of the surface tension force and the presence of the wall effect, the deflection profile of the swimmer differs from a sinusoidal wave and the swimmer does not swim as smoothly as it does on the water surface. Nevertheless, the swimmer is still able to swim under the water surface and its swimming direction can be roughly controlled in an open-loop fashion (See the supplementary video for underwater swimming demonstration).

## V. CONCLUSIONS

This work provides a mathematical model to describe the deflection profile of a flexible strip with a programmed magnetization profile in external uniform magnetic fields.

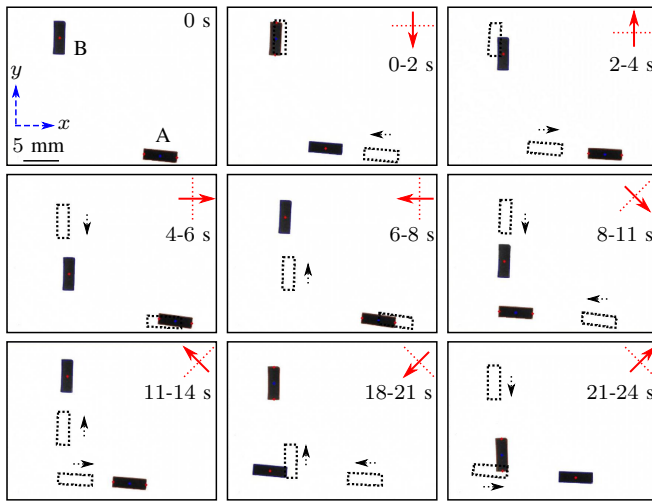


Fig. 7. Frames from a top-view video of the independent control of two swimmers on the water surface. The plane and direction of  $\mathbf{B}_a$  are indicated by dashed line segments and arrows, respectively. During this experiment,  $\mathbf{B}_{dc}$  always points towards positive  $x$  axis. Each image shows the swimmers' positions at two instances of time, with the preceding positions marked by dashed rectangles. Desired moving directions are labeled near the swimmer. Video is available in supplementary materials.

As a special case, the shape of a strip having a sinusoidal magnetization profile is studied, based on which, a swimmer is proposed that is capable of swimming in a non-holonomic fashion on or under the water surface in rotating uniform magnetic fields. Experimental deflection data shows a good agreement with the predictions made by the proposed mathematical model, suggesting that the model can accurately characterize the swimmer's deflection and be used to predict the swimmer's behavior and instruct the design of swimmers in different boundary conditions. Experimental results prove the swimmer's controllability and agility, and the possibility of independent multi-agent control. These results suggest that this type of swimmer has a promising potential to be applied in biomedical and microfluidic applications.

Different with the multi-agent control of helical swimmers demonstrated in [10], which employs the difference between the step-out frequencies of swimmers, the multi-agent control shown in this paper uses the difference between the directions of the swimmers' net magnetizations, and the complete independent control of the two swimmers are achieved. The proposed swimmer shares some capabilities with rigid helical swimmers, which are shown in [15] to be the likely best overall choice for in vivo biomedical applications. Both the proposed swimmer and helical swimmers move in a non-holonomic fashion, and reversing their swimming direction can be easily achieved by reversing the rotating direction of magnetic fields. In addition, both swimmers can be actuated with similar field generation systems.

The proposed swimmer differentiates itself from the others with its characteristics of being able to swim both on and below the fluid surface, and being propelled by the deflection

of its entire soft body, under the influence of rotating uniform magnetic fields. The entire body of the swimmer contributes to the magnetic and fluidic components of the propulsion, with no requirements for a head or tail. Future work will involve development of a more accurate model characterizing the swimming behavior based on related physical principles, and demonstration of 3D feedback control of the swimmer and additional multi-agent control capabilities.

## REFERENCES

- [1] E. Diller, and M. Sitti, "Micro-scale mobile robotics," *Foundations and Trends in Robotics*, vol. 2, no. 3, pp. 143-259, 2011.
- [2] S. Tottori, L. Zhang, F. Qiu, K. K. Krawczyk, A. Franco-Obregón, and B. J. Nelson, "Magnetic helical micromachines: Fabrication, controlled swimming, and cargo transport," *Adv. Mater.*, vol. 24, pp. 811-816, 2012.
- [3] E. Diller, and M. Sitti, "Three-dimensional programmable assembly by untethered magnetic robotic micro-grippers," *Adv. Funct. Mater.*, vol. 24, pp. 4397-4404, 2014.
- [4] B. J. Williams, S. V. Anand, J. Rajagopalan, and M. T. A. Saif, "A self-propelled biohybrid swimmer at low Reynolds number," *Nature Communications*, vol. 5, 2014.
- [5] A. A. Solovev, W. Xi, D. H. Gracias, S. M. Harazim, C. Deneke, S. Sanchez, and O. G. Schmidt, "Self-propelled nanotools," *ACS Nano*, vol. 6, pp. 1751-1756, 2012.
- [6] B. R. Donald, C. G. Levey, and I. Paprotny, "Planar microassembly by parallel actuation of MEMS microrobots," *J. Microelectromech. Syst.*, vol. 17, no. 4, 2008.
- [7] K. B. Yesin, K. Vollmers, and B. J. Nelson, "Modeling and control of untethered biomicrobots in a fluidic environment using electromagnetic fields," *Int. J. Robot. Res.*, vol. 25, no. 5-6, pp. 527-536, 2006.
- [8] K. E. Peyer, L. Zhang, and B. J. Nelson, "Bio-inspired magnetic swimming microrobots for biomedical applications," *Nanoscale*, 5, pp. 1259-1272, 2013.
- [9] L. Zhang, J. J. Abbott, L. Dong, B. E. Kratochvil, D. Bell, and B. J. Nelson, "Artificial bacterial flagella: Fabrication and magnetic control," *Appl. Phys. Lett.* 94, 064107, 2009.
- [10] A. W. Mahoney, N. D. Nelson, K. E. Peyer, B. J. Nelson, and J. J. Abbott, "Behavior of rotating magnetic microrobots above the step-out frequency with application to control of multi-microrobot systems," *Appl. Phys. Lett.* 104, 144101, 2014.
- [11] K. E. Peyer, E. Siringil, L. Zhang, and B. J. Nelson, "Magnetic polymer composite artificial bacterial flagella," *Bioinspir. Biomim.* 9, 046014, 2014.
- [12] I. S. M. Khalil, H. C. Dijkslag, L. Abelmann, and S. Misra, "Magnetosperm: A microrobot that navigates using weak magnetic fields," *Appl. Phys. Lett.*, 104, 223701, 2014.
- [13] R. Dreyfus, J. Baudry, M. L. Roper, M. Fermigier, H. A. Stone, and J. Bibette, "Microscopic artificial swimmers," *Nature*, vol. 437, pp. 862-865, 2005.
- [14] E. Diller, J. Zhuang, G. Z. Lum, M. R. Edwards, and M. Sitti, "Continuously-distributed magnetization profile for millimeter-scale elastometric undulatory swimming," *Appl. Phys. Lett.*, 104, 174101, 2014.
- [15] J. J. Abbott, K. E. Peyer, M. C. Lagomarsino, L. Zhang, L. Dong, I. K. Kaliakatsos, and B. J. Nelson, "How should microrobots swim?," *Int. J. Robot. Res.*, vol. 28, no. 11-12, pp. 1434-1447, 2009.
- [16] S. Palagi, E. Jager, B. Mazzolai, and L. Beccai, "Propulsion of swimming microrobots inspired by metachronal waves in ciliates: from biology to material specifications," *Bioinspir. Biomim.* 8, 046004, 2013.
- [17] N. T. Jafferis, H. Stone, and J. C. Sturm, "Traveling wave-induced aerodynamic propulsive forces using piezoelectrically deformed substrates," *Appl. Phys. Lett.*, 99, 114102, 2011.
- [18] J. B. Keller, "Surface tension force on a partly submerged body," *Phys. Fluids.*, vol. 10, no. 11, 1998.
- [19] G. Taylor, "Analysis of the swimming of microscopic organisms," *Proc. R. Soc. Lond. A*, vol. 209, pp. 447-461, 1951.